Supporting Information:

Coupling of Organic and Inorganic Vibrational States and Their Thermal Transport in Nanocrystal Arrays

Wee-Liat Ong[†], Shubhaditya Majumdar[†], Jonathan A. Malen[†‡], Alan J. H. McGaughey[†‡]*

†Department of Mechanical Engineering, Carnegie Mellon University, 5000 Forbes Ave, Pittsburgh, PA 15213

‡Department of Materials Science and Engineering, Carnegie Mellon University, 5000 Forbes Ave, Pittsburgh, PA 15213

Corresponding Author

*E-mail: mcgaughey@cmu.edu

I Inter- and Intra-molecular Potentials

The dodecanethiol ligands are modeled using the Hautman-Klein united atom model.[1] Bond stretching, bending, and torsional potentials govern the bonded interactions within a ligand. The light hydrogen atoms in the ligand backbone are treated implicitly with their masses lumped into the corresponding carbon atoms. Such a simplification reduces computational cost as less atoms and a bigger molecular dynamics (MD) timestep can be used without compromising the MD accuracy for geometrical packing [1–3] and thermal conductivity [4–6] studies at room temperature. The high vibrational activation temperature of the stiff C-H bond justifies this simplification. Notwithstanding, these lumped hydrogen atoms are spatially accounted for in the potentials, mimicking the steric effect of the hydrogen atoms.[1] A Morse potential dictates the interaction between the S atoms and the Au cores.[7,8] Lennard-Jones (LJ) potentials and the Lorentz–Berthelot mixing rules[9] are used to model long-range inter- and intra-(CH_2, CH_3, and S sites in the same ligand that are at least four bonds away) molecular interactions. The cut-off distance for the Morse and LJ potentials is set at 10 A. An embedded atom model (EAM) potential[10] is used for the Au atoms as it matches the experimental bulk phonon density of states better than a simple Au Morse potential.[11] The potentials and parameters[2,5,10] used are provided in Table S1.

Table S1. Potentials and their parameters

Potential	Type	Parameters
Bond Stretching[2] $E_s = \frac{1}{2} k_s (r - r_o)^2$	S-C C-C	k_s = 9.627 eV/A^2, r_o = 1.815 A k_s = 11.27 eV/A^2, r_o = 1.54 A

Bond Bending[5] $E_\theta = \frac{1}{2}k_\theta(\theta - \theta_o)^2$	S-C-C C-C-C	k_θ = 5.388 eV/rad^2, θ_o = 114.4° k_θ = 5.388 eV/rad^2, θ_o = 109.5°
Dihedral[5] Ryckaert–Bellemans $E_D = \sum_{i=0}^{5} a_i \cos^i \phi$	C-C-C-C S-C-C-C (same for both)	a_0 = 0.09617 eV, a_1 = -0.125988 eV, a_2 = -0.13598 eV, a_3 = 0.0317 eV, a_4= 0.27196 eV, a_5= 0.32642 eV
Lennard-Jones[5] with Lorentz–Berthelot mixing rules $E_{LJ} = 4\varepsilon_{ij}\left[\left(\frac{\sigma_{ij}}{r_{ij}}\right)^{12} - \left(\frac{\sigma_{ij}}{r_{ij}}\right)^{6}\right]$, where *i* and *j* refer to different atom types.	Au CH_3 CH_2 S (with CH_3 and CH_2) S (with other S)	ε = 0.00169 eV, σ = 2.935 A ε = 0.00759 eV, σ = 3.905 A ε = 0.00512 eV, σ = 3.905 A ε = 0.01086 eV, σ = 3.55 A ε = 0.01724 eV, σ = 4.25 A
Morse[5] $E_{morse} = D_e\left[\left(1 - e^{-a(r-r_m)}\right)^2 - 1\right]$	Au-S	D_e = 0.38 eV a = 1.47 A^{-1} r_m = 2.65 A
EAM potentials[10]	Au-Au	

II NCA Simulation Details

All MD simulations were performed using LAMMPS[12] with a time step of 1 fs. Periodic boundary conditions in the three Cartesian directions were implemented in all simulations except during the determination of NCA thermal conductivity, where nanocrystals are fixed along the two boundaries in the direction of heat flow (Figure 1e).

The NCA thermal conductivity (k_{NCA}) is predicted using the direct method under non-equilibrium molecular dynamics (NEMD) simulation.[13] NCAs of desired thickness (10 to 90 nm, requiring between 30,000 to 300,000 atoms) were thermalized at a temperature of 300 K for 1 ns using velocity rescaling and equilibrated for a further 1 ns under the microcanonical ensemble before the start of the direct method. By randomizing the initial velocity for each atom, any artificial periodicity in the NCA created during the duplication and stacking of the unit cell is removed. During the direct method simulations, a heat flow was induced through the NCA by sourcing and sinking a predetermined amount of heat ($\vec{q}$ ranging from 0.075 to 0.31 eV/ps) at the source and sink regions (Figure 1e) for a total time of 20 – 40 ns. Only the cores were used to source and sink heat as a few (5 to 8) ligands can dislodge and bond to other cores during the simulations. The targeted steady state temperature difference between region L_1 and L_n is 30 ± 10 K (i.e., 10 % of average simulation temperature). The thicker the NCA, the longer it takes to reach steady-state – a condition determined by comparing the time-averaged temperature profile after each nanosecond. A layer's (as depicted in Figure 1e) temperature is obtained by averaging all core temperatures in that layer (core-to-core temperature variation < 1 %). The resulting steady-state temperature gradient ($\frac{dT}{dx}$) between region L_1 and L_n, obtained by averaging blocks of 1 ns for a total duration of 10 ns, was used

in the Fourier law ($\vec{q} = -k_{NCA} A \frac{dT}{dx}$, where A is the area perpendicular to the heat flow) to obtain the thermal conductivity.

III Thickness- and Core Diameter-dependent NCA Thermal Conductivity

We first determined the cross-sectional area required to get converged thermal conductivity predictions. Using an NCA of 9 nm in thickness built from cores of 1.6 nm in diameter, thermal conductivity predictions were made using three progressively larger cross-sectional areas. As shown in Table S2, all systems predict a value at 0.16 W/m-K, indicating the suitability of the smallest model (i.e., cross-sectional area of 32.86 nm^2, 2 x 2 nanocrystals). The 2 x 2 nanocrystal cross section is used for all diameters.

Table S2. Simulated NCA thermal conductivity for cross-sectional area convergence for 1.6 nm diameter nanocrystals.

Cross-sectional Area (nm^2)	Thermal conductivity (W/m-K)
32.85	0.166
65.71	0.159
131.43	0.163

We validate our full-scale NCA model by comparing the thickness- and core diameter-dependence of thermal conductivity with experimental measurements.[14] For the thickness series, thermal conductivities of NCAs built using cores of 1.6 nm and 4.0 nm in diameter were predicted for thicknesses between 9 and 90 nm. The results are plotted alongside experimental measurements for a 4.5 nm core gold NCA of similar film thicknesses in Figure 2. Both simulation and experiment show a thickness-invariant thermal conductivity with similar magnitudes. This invariance indicates diffusive thermal transport in the NCAs with scattering from the boundaries playing a negligible role.[14]

Given the thickness-invariance of the thermal conductivity, the diameter series was performed using the minimum number of layers (three) required to establish a steady-state temperature gradient during the direct method simulation. The thermal conductivity

predictions for six different core diameters and the single 4.5 nm gold core experimental point are plotted in Figure 4b. The simulations show an increasing thermal conductivity trend when the diameter is larger than 2 nm, capturing the upward experimental trend we measured for PbS, PbSe, PbTe, CdSe, and Fe_3O_4 NCAs.[14] In addition, the predicted magnitude for a diameter of 4.5 nm is within the uncertainty of the corresponding experimental measurement. It is thus evident that the full-scale NCA model captures both the magnitude and trend of the existing experimental measurements well, giving confidence to the chosen potentials and their extension to future predictions.[15,16]

IV Gold Thermal Conductivity from Molecular Dynamics

The gold bulk thermal conductivity was predicted using the NEMD technique. A block of gold with dimensions 26x25x174 A^3 (corresponding to 6750 atoms) was used for the simulations. Periodic boundary conditions were imposed in the *x*- and *y*-directions. Fixed boundary conditions were imposed in the *z*-direction, which is the [111] direction for the FCC gold crystal structure and the direction for simulating the heat flow. The two layers adjacent to each fixed boundary were used as the heat source and heat sink. The interatomic gold potential used is referenced in Table S1. The system was first relaxed in the canonical ensemble at a temperature of 300 K for 1.5 ns. After this equilibration, the NEMD algorithm was started in the microcanonical ensemble with a heat flow of 0.0001 eV/fs. The temperature of the gold atoms was collected after an initialization period of 2.5 ns for a period of 7 ns. This time period was determined to be adequate for reaching steady state. The gold atoms were divided into 22 temperature regions (each region consisting of 3 layers of gold with 270 atoms). The slope of the temperature profile was calculated and used in the Fourier law to predict the gold bulk thermal conductivity. Table S3 gives the predicted values

with respect to the mass, *M*, of the gold atoms, which was varied for use in the core mass series. We note that, as expected, the thermal conductivity scales according to $\frac{1}{\sqrt{M}}$.[17]

Table S3. Thermal conductivity of bulk gold with different mass multiples from molecular dynamics.

M/M_{Au}	K (W/m^2-K)
0.01	17.4
0.05	7.86
0.3	3.08
1	1.84
2	1.27
4	0.94
8	0.67
16	0.47

V Dodecanethiol Solid Thermal Conductivity from Molecular Dynamics

The thermal conductivity of a dodecanethiol solid is obtained using the NEMD technique in LAMMPS and the appropriate potentials as defined in Table S1. A block of randomly arranged dodecanethiol ligands (23933 atoms using the united atom approach) was first thermalized at a temperature of 300 K for 1 ns using velocity rescaling and equilibrated for a further 1 ns under the microcanonical ensemble with periodic boundary conditions. This block of ligands was then subjected to an isothermal-isobaric ensemble at an average temperature of 300 K and pressure of 0 Pa for 1 ns to obtain an equilibrium liquid. This resulting liquid has a density of 0.85 g/cm^3, which agrees well with the experimental value of 0.84 g/cm^3.[18] To obtain a well-ordered solid near to room temperature, the liquid is first cooled at a rate of 1 K/ns to an average system temperature of 150 K before reheating and thermalizing to 300 K under the canonical ensemble for 1 ns followed by microcanonical ensemble for another 1 ns. The NEMD method was implemented at this temperature by fixing the two ends of the solid and dividing the solid into five regions, each of thickness 3

nm. Two of these regions were used to source and sink heat (0.08 eV/fs) through the remaining regions to achieve a target ΔT of approximately 10% of the average temperature. The steady state temperature profile was obtained by averaging blocks for 1 ns for a total duration of 10 ns and was used in the Fourier's law to obtain the ligand thermal conductivity. The ligand solid thermal conductivity at an average temperature of 300 K is 0.15 ± 0.01 W/m-K.

VI Molecular Dynamics Prediction of SAM Interfacial Thermal Conductance

The $h_{SAM/gold}$ value was predicted by implementing NEMD on a gold-SAM-gold junction (Figure S1). To setup the system, decanedithiol ($C_{10}H_{21}SH$) molecules were first placed on the (111) face of a gold block having dimensions of 25x24x60 A^3 (2160 atoms). The alkanethiol SAMs were populated on the gold surface with a coverage density of 21.6 A^2 per molecule and placed close to the surface FCC sites in the experimentally observed $(\sqrt{3}x\sqrt{3})R30^o$ configuration.[19] The potentials used are found in Table S1. This system was first equilibrated in the canonical ensemble for 1.5 ns. After this equilibration, a second gold block (identical in dimensions to the first gold block) was placed on the other side of the SAM. This entire junction was then equilibrated for a further 1.5 ns. After this, a heat flow of 0.0001 eV/fs was added/removed for the heat source/sink (consisting of 180 atoms each) located next to the fixed ends (90 atoms each) of either gold block. Steady-state temperature data was collected for all the atoms after 2.5 ns for a period of 20 ns. The temperature gradient in each of the two gold blocks was obtained by fitting a line through eight successive temperature points - each the average temperature of three layers of atoms (270 atoms). Since a strong non-linearity in the temperature profile could be seen at the edge of a SAM/gold interface, the temperature difference was determined at the point where the profile in each gold block became linear. On average, this location was three to five layers of gold atoms away from the physical SAM/gold interface. The number of temperature points considered in the fit was varied from five to seven. Using more points captures the non-linear sections of the temperature profile near the gold-SAM interface. The interfacial thermal conductance of gold/SAM/gold was predicted by dividing the imposed heat flow by the average of the three temperature differences. The predicted value for the gold/SAM/gold junction is 110 ± 10 MW/m^2-K. By assuming a negligible thermal resistance contribution from the molecules and that the individual interfacial thermal conductances of the two

interfaces are non-interacting and in series, a single SAM/gold interface will have an interfacial thermal conductance value of 220 ± 20 MW/m^2-K. Although this value is obtained using decanedithiol instead of dodecanedithiol molecules, the SAM interfacial thermal conductance has been found to be invariant with the molecule length.[5,11,16]

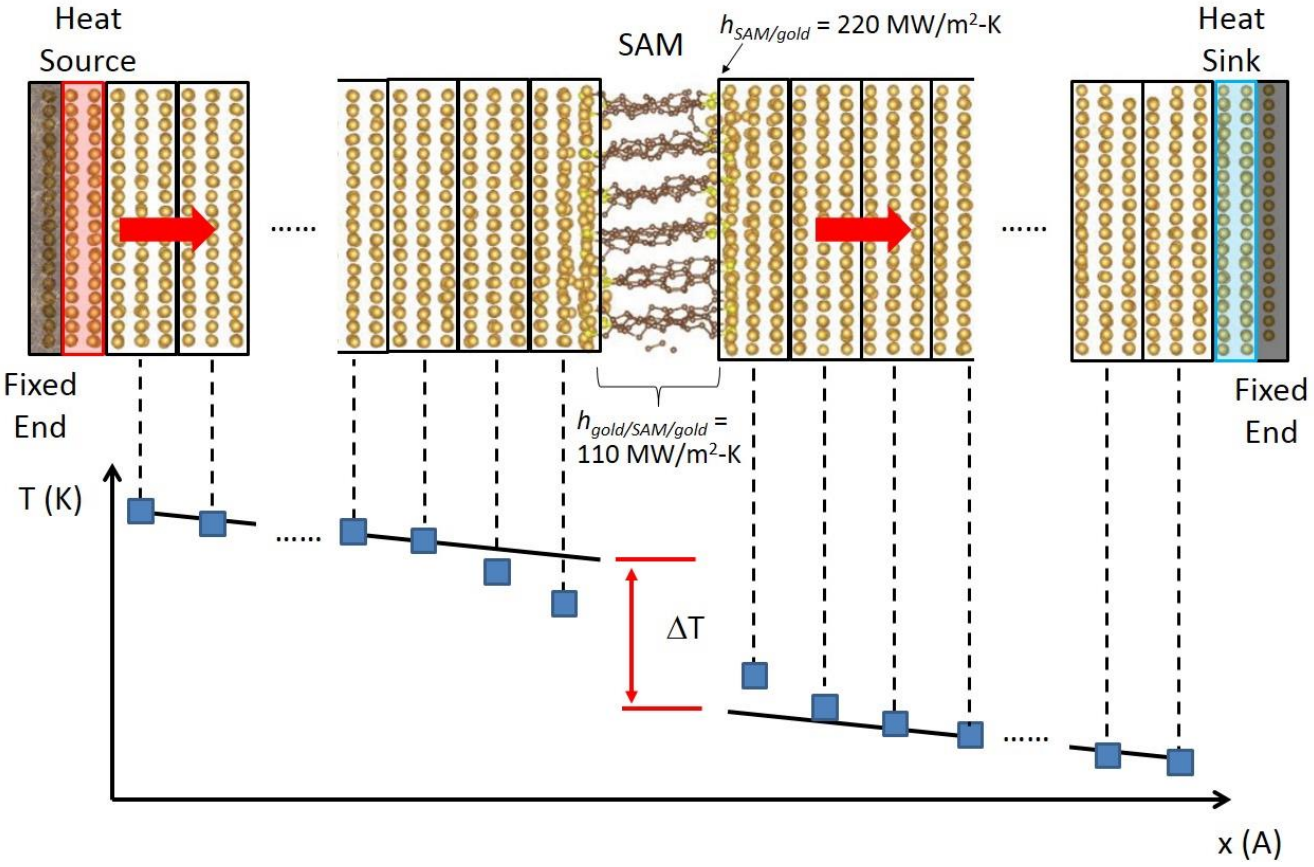

Figure S1. SAM junction used for predicting the interfacial thermal conductance. A representative temperature profile and the fits are shown below.

VII Uncertainty Analysis

In Figure 2, the error bar comes from standard deviation of repeated measurements of the core diameters. In Figures 3 and 4, the error bar on individual data point is the standard

deviation from the five consecutive average of blocks of 1 ns simulation after steady state was reached.

In Figure 3a, the uncertainty in $h_{SAM/gold}$ is twice the standard deviation obtained from the thermal conductance prediction of the gold/SAM/gold junction.

The uncertainty for predictions made using eq 4 comes purely from the uncertainty of $h_{SAM/gold}$. In Figure 3b, the uncertainty associated for values calculated from eq 3 comes from the uncertainties in three of the individual inputs (i.e., k_m, k_p, and h), which are combined using a root-sum of difference-square method.[20]

References

(1) Hautman, J.; Klein, M. L. Simulation of a Monolayer of Alkyl Thiol Chains. *J. Chem. Phys.* **1989**, *91*, 4994.

(2) Ghorai, P. K.; Glotzer, S. C. Molecular Dynamics Simulation Study of Self-Assembled Monolayers of Alkanethiol Surfactants on Spherical Gold Nanoparticles. *J. Phys. Chem. C* **2007**, *111*, 15857–15862.

(3) Kaushik, A. P.; Clancy, P. Solvent-Driven Symmetry of Self-Assembled Nanocrystal Superlattices-a Computational Study. *J. Comp. Chem.* **2013**, *34*, 523–32.

(4) Luo, T.; Lloyd, J. R. Non-Equilibrium Molecular Dynamics Study of Thermal Energy Transport in Au–SAM–Au Junctions. *Int. J. Heat Mass Transf.* **2010**, *53*, 1–11.

(5) Luo, T.; Lloyd, J. R. Equilibrium Molecular Dynamics Study of Lattice Thermal Conductivity/Conductance of Au-SAM-Au Junctions. *J. Heat Transf.* **2010**, *132*, 032401.

(6) Babaei, H.; Keblinski, P.; Khodadadi, J. M. Thermal Conductivity Enhancement of Paraffins by Increasing the Alignment of Molecules through Adding CNT/graphene. *Int. J. Heat Mass Transf.* **2013**, *58*, 209–216.

(7) Sung, I.-H.; Kim, D.-E. Molecular Dynamics Simulation Study of the Nano-Wear Characteristics of Alkanethiol Self-Assembled Monolayers. *Appl. Phys. A* **2004**, *81*, 109–114.

(8) Mahaffy, R.; Bhatia, R.; Garrison, B. J. Diffusion of a Butanethiolate Molecule on a Au{111} Surface. *J. Phys. Chem. B* **1997**, *101*, 771–773.

(9) Allen, M. P.; Tildesley, D. J. *Computer Simulation of Liquids*; Clarendon Press: Oxford, 1987.

(10) Grochola, G.; Russo, S. P.; Snook, I. K. On Fitting a Gold Embedded Atom Method Potential Using the Force Matching Method. *J. Chem. Phys.* **2005**, *123*, 204719.

(11) Duda, J. C.; Saltonstall, C. B.; Norris, P. M.; Hopkins, P. E. Assessment and Prediction of Thermal Transport at Solid-Self-Assembled Monolayer Junctions. *J. Chem. Phys.* **2011**, *134*, 094704.

(12) Plimpton, S. Fast Parallel Algorithms for Short-Range Molecular Dynamics. *J. Comp. Phys.* **1995**, *117*, 1–19.

(13) Schelling, P. K.; Phillpot, S. R.; Keblinski, P. Comparison of Atomic-Level Simulation Methods for Computing Thermal Conductivity. *Phys. Rev. B* **2002**, *65*, 144306.

(14) Ong, W.-L.; Rupich, S. M.; Talapin, D. V.; McGaughey, A. J. H.; Malen, J. A. Surface Chemistry Mediates Thermal Transport in Three-Dimensional Nanocrystal Arrays. *Nat. Mater.* **2013**, *12*, 410–5.

(15) Losego, M. D.; Grady, M. E.; Sottos, N. R.; Cahill, D. G.; Braun, P. V. Effects of Chemical Bonding on Heat Transport Across Interfaces. *Nat. Mater.* **2012**, *11*, 502–6.

(16) Wang, R. Y.; Segalman, R. A.; Majumdar, A. Room Temperature Thermal Conductance of Alkanedithiol Self-Assembled Monolayers. *Appl. Phys. Lett.* **2006**, *89*, 173113.

(17) McGaughey, A.; Hussein, M.; Landry, E.; Kaviany, M.; Hulbert, G. Phonon Band Structure and Thermal Transport Correlation in a Layered Diatomic Crystal. *Phys. Rev. B* **2006**, *74*, 1–12.

(18) *Handbook of Data on Organic Compounds*; Lide, D. R.; Milne, G. W. A., Eds.; 3rd ed.; CRC Press, Inc: Boca Raton ,FL., 1994; p. 2545.

(19) Strong, L.; Whitesides, G. M. Structures of Self-Assembled Monolayer Films of Organosulfur Compounds Adsorbed on Gold Single Crystals: Electron Diffraction Studies. *Langmuir* **1988**, *4*, 546–558.

(20) Malen, J. A.; Baheti, K.; Tong, T.; Zhao, Y.; Hudgings, J. A.; Majumdar, A. Optical Measurement of Thermal Conductivity Using Fiber Aligned Frequency Domain Thermoreflectance. *J. Heat Transf.* **2011**, *133*, 081601.